XYZ robotic positioning of 3D microcomponents at the tip of an AFM cantilever

Morris Mwangi[1,2], Miguel Suarez[2], Roland Salut[2], Freddy Romero Leiro[2], Jean Bosco Byiringiro[1], Nadège Courjal[2] and Cédric Clévy[2]

***Abstract*— This article deals with the realization of 3D and precise positioning tasks of components at the micrometric scale using robots. This scale is characterized by the predominance of surface forces that are difficult to predict, inducing huge challenges to accurately position two components. In this article, a hybrid vision-force robotic strategy is studied combining a planar positioning by vision associated with visual features and an out-of-plane positioning exploiting the real time measurement of these forces with an Atomic Force Microscope (AFM). This approach aims at achieving precise positioning in 3D and in a generic way because it can apply to a wide variety of components and tasks as long as one of the components can be mounted on an AFM cantilever. The experimental validation is carried out in a case study consisting of positioning nanophotonic components of a few tens of micrometers in typical dimensions. The results show that the proposed robotic strategy is repeatable and, to our knowledge, achieves a positioning precision of 23 nm along Z for the first time. This work opens unique and key perspectives in terms of material hybridization and component configurations such as possible out-of-plane positioning.**

I. Introduction

The assembly of complex three-dimensional microscale architectures by combining individual components is an attractive approach for integrating heterogeneous materials and functional building blocks into advanced systems. However, assembling components with characteristic dimensions ranging from a few micrometers to several hundreds of micrometers presents significant challenges. At this scale, physical interactions between components become dominant during manipulation and assembly. These interactions include both short-range contact forces and longer-range forces arising from adhesion, capillary effects, van der Waals interactions, and electrostatic forces[1]. Such scale effects can strongly influence the behaviour of microscale components and may lead to unintended sticking, unstable contact, or damage to fragile structures. Moreover, the magnitude and behaviour of these forces depend on several factors such as surface quality, geometry, environmental conditions, and the sequence of manipulation steps [2]. As a result, these interaction forces remain difficult to model and predict, particularly during complex robotic assembly processes involving multiple tasks and components.

Several approaches have been proposed to address microscale assembly challenges. One strategy involves dedicated robotic tools designed to manage adhesion during gripping and release [3], [4], [5]. While these specialized tools show promising results, they are often designed for particular component geometries or material properties, which limits their versatility for assembling diverse microscale structures.

A second widely adopted approach consists of measuring interaction forces during manipulation and using them in closed-loop control to adapt the robot behaviour in real time. By monitoring tool–component forces, the system can regulate motion to maintain stability and achieve high precision [6], [7], [8], [9], [10].

Although these strategies demonstrate high precision and versatility in 3D assembly, they are often limited to components of several hundred micrometers due to bulky manipulation tools or task-specific system designs such as using an optical feedback for optical components assembly (active alignement principle).

Atomic Force Microscopes (AFM) provide a promising solution for microscale assembly due to their high force sensitivity and nanometric positioning capability. AFM-based manipulation has demonstrated potential for precise robotic tasks at the micro- and nanoscale. For example, [11] achieved automated 3D pick-and-place manipulation of 3-4 μm microspheres using a nano-tip gripper composed of two independently actuated AFM cantilevers with optical force feedback, where pull-in and pull-off forces indicated contact states and cantilever deflection estimated transport forces. Other works have explored AFM-based robotic strategies such as micrometric sample rotation around the AFM tip [12], trajectory-based positioning with about 1 nm accuracy [13], and hybrid control combined with Scanning Electron Microscope (SEM) imaging for component characterization and manipulation [14]. Although many of these studies focus on surface characterization, they demonstrate the strong potential of AFM systems for high-precision 3D robotic manipulation while accounting for interaction forces.

Despite these advances, a generic approach for out-of-plane three-dimensional nanopositioning of microscale components remains necessary. To address this challenge, the present work proposes an approach in which the component

*This work was supported by EIPHI Graduate School under grant agreement "ANR-17-EURE-0002", Bourgogne Franche-Comte region, the ANR Dynabot (contract "ANR-21-CE10-0016") and the French RENATECH and ROBOTEX networks (TIRREX ANR-21-ESRE-0015) through their FEMTO-ST technological facilities MIMENTO and CMNR.

[1]Morris Mwangi and Jean Bosco Byiringiro are with Dedan Kimathi University of Technology, Department of Mechatronic Engineering, Nyeri - Kenya. morris.mwangi@dkut.ac.ke

[2]Morris Mwangi, Miguel Suarez, Roland Salut, Freddy Romero Leiro, Nadège Courjal and Cédric Clévy (IEEE Senior Member) are with Université Marie et Louis Pasteur, SUPMICROTECH, CNRS, FEMTO-ST Institute, F-25000 Besancon, France. cclevy@femto-st.fr

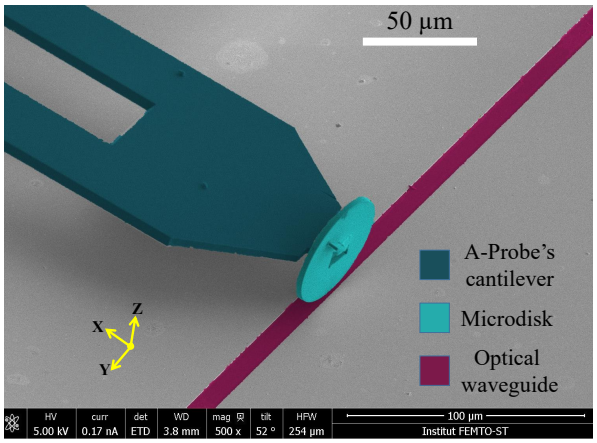


Fig. 1. 3D Positioning of photonic components (a $50\mu m$ diameter disk relative to an optical waveguide) using a robotic approach based on AFM.

to be positioned is mounted directly on the tip of an AFM cantilever, as illustrated in Fig. 1. The relative positioning between the components is then achieved using a hybrid vision–force robotic strategy. In this approach, planar alignment in the X–Y plane is performed using visual feedback and identifiable features on the components, while the out-of-plane positioning along the Z-axis exploits the force sensing capabilities of the AFM cantilever. This strategy combines the advantages of optical localization and high-sensitivity force detection, providing a versatile framework that can be applied to a wide variety of microscale components.

To experimentally investigate the proposed approach, this work focuses on the positioning of photonic components, specifically the alignment of a microdisk with a lithium niobate (LN) optical waveguide to form an optical ring resonator [15]. Such resonators are widely used in photonic systems due to their compact size and high performance. However, their assembly remains challenging because of the stringent positioning requirements and the strong interaction forces that arise at this scale. Due to these challenges these resonators are manufactured using monolithic approaches [16]. The proposed AFM-based robotic positioning framework aims to address these challenges by enabling high-precision three-dimensional alignment and controlled contact between microscale photonic components.

II. Assembly of the Microdisk on AFM Cantilever by Tele-Operation

A microrobotic strategy based on Atomic Force Microscopy (AFM) is proposed to control the relative positioning of microscale components. A microdisk resonator is considered as a case study for an optical ring resonator configuration, where the microdisk is brought close to a suspended LN waveguide. The microdisk is mounted on a cantilever and vertically positioned relative to the waveguide (Fig. 1). This vertical coupling configuration enables selective optical filtering and high-sensitivity sensing while providing a modular platform for integrated photonics. It is also used to study intermolecular interaction forces and 3D positioning between components. This section therefore presents the assembly of the microdisk on an AFM cantilever by teleoperation under SEM.

For 3D microassembly, high-resolution optical microscopy combined with a precision microgripper is employed for accurate visualization and manipulation of components. However, intrinsic microscale variability and poorly controlled interaction forces complicate pick-and-place operations in air, motivating the use of force-control strategies [1]. In this work, assembly is therefore conducted under vacuum conditions to improve stability and reduce environmental disturbances. Despite these measures, the process remains demanding, requiring skilled operation to achieve precise positioning while preventing damage to both the microcomponents and the manipulation tool.

Fig. 2 shows the internal view of a SEM/FIB dualbeam Helios nanolab 600i from Thermofisher upgraded with multiple Gas Injection System (GIS) dedicated for in-situ deposition (Pt, C) used for the assembly. The micromanipulator Kleindiek MM3A can operate in the SEM chamber and is upgraded with a rotation axis RoTip and a microgripper MGS2.

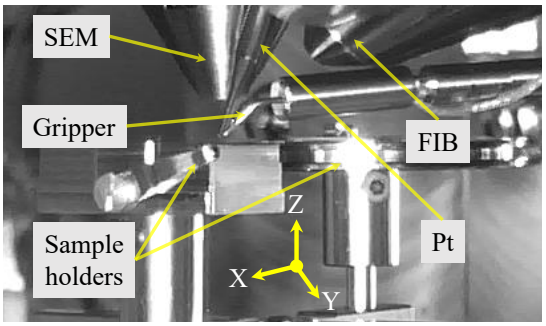


Fig. 2. Internal view of the Scanning Electron Microscope (SEM) chamber that includes several tools: A microgripper, SEM & Focused Ion Beam (FIB) for visualization, FIB for additive or substractive manufacturing. Platinum (Pt) is the material for deposition.

This complete platform enables the tele-operation of the assembly process since (1) it enables a 3D view of the sample, (2) it can mill a wide range of materials like silicon or LN, (3) it is able to deposit Carbon or Platinum to add material in a specific area or to solder two elements and (4) it can manipulate micro-components in 6 degrees of freedom.

Fig. 3 illustrates the main steps in the assembly of the microdisk at the tip of an AFM cantilever. First, the microdisk is prepared by FIB milling on a X-cut $LiNbO_3$ membrane with a 1 µm thickness. The microdisk edges are patterned by a 30 kV - 9 nA beam and then polished at 30 kV - 2.5 nA. Three small tabs are left around the disc pending the next step. The AFM cantilever (NT-MDT, CSG10) is also prepared by FIB milling (30 kV - 9 nA) with a specific shape consisting in a tip on which the disk will be plugged. Custom made sample holders have been designed and fabricated to handle the two samples in predetermined orientation inside the chamber. Since the positions of the SEM and FIB columns and also that of the micromanipulator

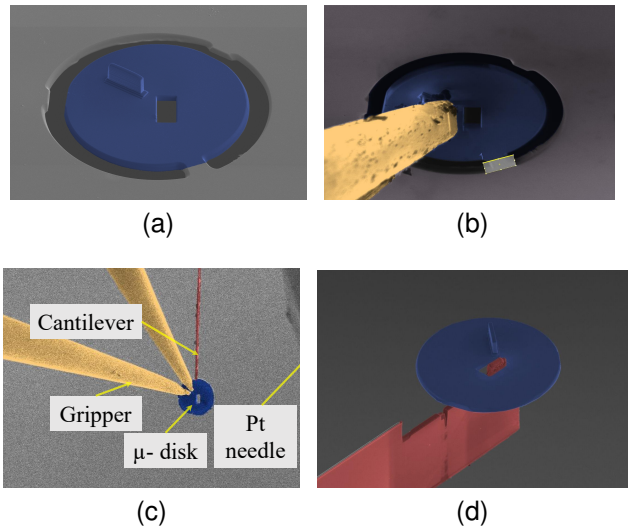


Fig. 3. Images showing the assembly of the microdisk on an AFM cantilever. The diameter of the microdisk = ∼50 µm (a) Deposition of Carbon holding tab and milling of a hole for insertion of the cantilever. (b) Gripping of the microdisk and detachment by FIB milling. (c) View of the microgripper and the microdisk during Pt deposition. (d) Close view of the assembled microdisk on the AFM cantilever.

and of the GIS are fixed, everything must be organized for perfect operability while avoiding collisions.

In a second step, a Carbon (C)-tab is deposited at the center of the microdisk at 30 kV - 230 pA and a square hole is milled close to the tab at 30 kV - 790 pA. An active zone of 32 µm is kept all around the wafer to avoid any interference with the optical signal. Two of the three tabs are milled and the microdisk is then held using the microgripper thanks to the C-tab as shown by Fig. 3a. The last tab is finally cut and the stage lowered to recover the microdisk (Fig. 3b). The most critical step is to then bring the AFM cantilever pin to the existing hole in the disk. The disk has to be perfectly aligned in the coincidence point of SEM and FIB to get the 3D view and to be as precise as possible. When the correct position is reached, the microdisk is soldered to the AFM cantilever and is finally released as illustrated by Fig. 3c. The final step consists in a polishing step at 30 kV-2.5 nA to remove the defects left by the 3 tabs (Fig. 3d). The C-tab is left as it not in the active zone of the microdisk.

III. Experimental set-up for XYZ positioning and measurement of interaction forces

The experimental setup (Fig. 4) comprises a regular AFM (SMENA B:SFC100) equipped with a Z-axis mechanical screw for coarse positioning (range 2 cm, resolution 1.8 µm) and a piezo-electric positioner on which the AFM tip is mounted for high-resolution 3D scanning (X/Y range 40 µm, Z range 6 µm). A Position Sensitive Device (PSD) measures cantilever deflection (laser intensity) and the AFM can operate in open-loop or closed-loop (PSD feedback) modes; in closed-loop a setpoint on the AFM interface defines the contact force and a PID controller automatically adjusts the piezo Z to nullify force error.

For sample/microdisk alignment additional positioners are placed under the sample holder: a PI XY micro-positioner (M-545.2MN, 1 µm resolution, 25 mm travel per axis) for coarse waveguide displacement, and a PI XYZ nanopositioner (P-733.3 DD, 0.1 nm resolution; X/Y range 30 µm, Z range 10 µm) with integrated capacitive sensors for closed-loop, high-accuracy positioning. Visual localization is provided by an inverted microscope with a $\times 20$ objective; because the waveguide is LN which is transparent the microdisk can be observed through the waveguide. The waveguide is connected to the optical signal measurement as shown in the control scheme in Fig. 5.

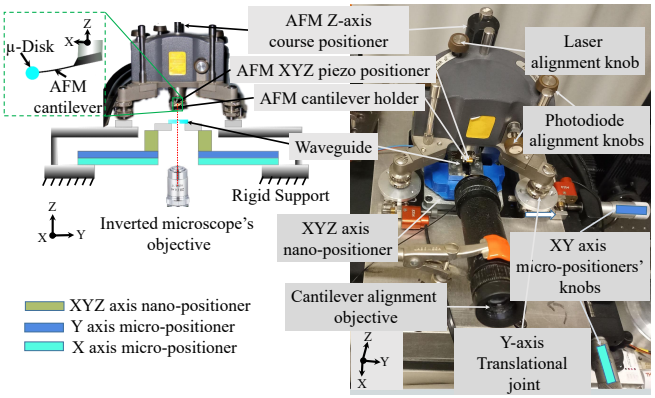


Fig. 4. The experimental set-up showing the key positioning stages used in the study of the optical and physical interaction of the between the waveguide and the microdisk.

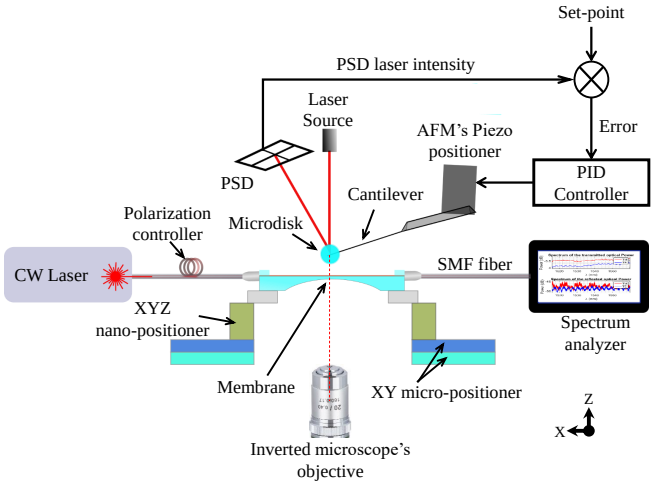


Fig. 5. Scheme of the control diagram for the experimental set-up for optical response measurements.

IV. Robotic strategy for positioning of the waveguide and the microdisk in X and Y axes

A visual-based approach is developed to position the microdisk along X and Y of the waveguide using an inverted microscope. Because it is practically impossible to put visual references (patterns) on the microdisk, this is done on the waveguide's surface. This involves adapting the manufacturing process of the waveguide to facilitate the positioning of

the microdisk on the waveguide (along the Y-axis) at the waveguides thin section (along the X-axis).

Fig. 6 shows an image of the top view of the waveguide after the membrane was engraved with an optical grade dicing saw. The purpose here is to test the spectral response of the interaction between the waveguide and the microdisk at the thinnest section of the waveguide, which enhances the electro-optical properties of the waveguide and the evanescent field coupling between the waveguide and the microdisk.

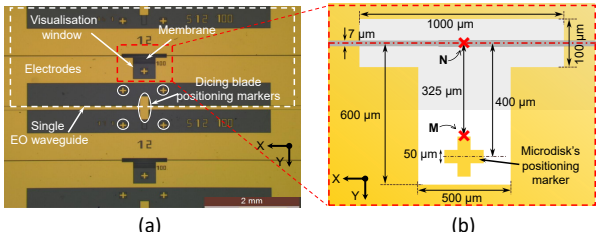


Fig. 6. Key features for positioning of the microdisk with respect to the waveguide at the thinnest section of the membrane. (a) Picture showing the top view of the fabricated waveguides after engraving of the membranes. (b) Zoomed view of the visualization window showing detailed dimension of key features for relative positioning of the microdisk with respect to the waveguide.

The transparency of the $LiNbO_3$ material used for the fabrication of the waveguide contributes to the positioning of the microdisk. However, the deposition of electrodes for electro-optical modulation hinders the visibility through them. Therefore, a visualization window is placed on the waveguide to enable the visibility of the microdisk through it during initial positioning. However, the precise position of the thinnest section cannot be inferred visually. Therefore, to locate the thin section, a positioning marker (microdisk positioning marker) is placed on the waveguide during electrode deposition. Additionally, the microdisk positioning marker gives the precise distance to facilitate the location of the optical waveguide as shown in the scheme of Fig. 6.

Finally, to position the microdisk at the point N of Fig. 6 (325 µm from point M), the waveguide is moved using the nanopositioner along the Y-axis.

V. Repeatability Test on Contact Detection and Interaction Force Estimate along Z

To quantify the repeatability in positioning and understand the interaction behavior between the microdisk and a waveguide along Z based on AFM measurement, two sets of experiments are performed. The first set involves an AFM tip (which serves as a reference for comparison of the behavior) and the sample (which will have a similar effect as the waveguide because they are fabricated from the same material), and the second set involves the microdisk and the sample.

For each case, the sample is approached and retracted from a fixed AFM cantilever (with the tip/microdisk) at a constant speed of (100 nm/s) and the AFMs laser intensity is recorded. It should be noted that the sample displacement range during each experiment is kept constant, i.e. 2 µm, which helps to maintain the preload force at a manageable tolerance, thus enabling understanding of the dynamics of the interaction when making several tests.

A. Study on the behavior of the AFM tip-sample interaction

Fig. 7 shows a set of ten force-displacement curves, showing the behavior of an AFM cantilever (NT-MDT CSG10) with a stiffness constant of 0.1 N/m on an $LiNbO_3$ sample.

The pull-in and pull-off data from each approach and retract curve are recorded with their respective positions, in table I, to analyze the repeatability of: first, the magnitude of the pull-in and pull-off forces and the corresponding positions. Second, the time it takes from no contact to contact for the pull-in and contact to no contact for the pull-off forces.

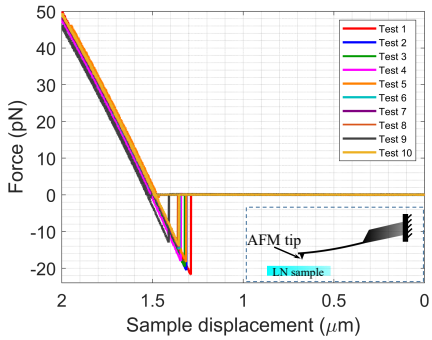


Fig. 7. Experimental results showing 10 force-displacement curves (usually we name these "approach-retract" curves) used in the estimation of pull-in and pull-off forces during AFM tip/LN sample interaction.

The pull-in force increases with the decrease in the distance between the sample and the tip. With this in mind, the maximum pull-in force is reached when the distance between the sample and the tip is minimum. Therefore, we can consider contact at this point. From the results, the maximum pull-in forces are detected with a standard deviation of 13 nm. This implies a highly repeatable detection of the sample surface based on the pull-in forces in contact. Indeed, if the pull-in forces are detected earlier before reaching the maximum value, this can be used as a non-contact way of predicting the sample position, similar to the non-contact mode AFM.

The mean and standard deviations of the respective maximum forces and the corresponding events (pull-in or pull-off) duration and positions are used to analyze behavior. From the results in Table I, the mean value of the pull-off forces is $\sim$19 times higher than that of the pull-in forces. This is expected as a result of the increased adhesion of the tip to the sample surface after contact because the experiments are done under ambient conditions. When the tip gets in contact with the sample, the capillary forces caused by the thin water film on the sample surface bind to the contact, increasing the tip-sample adhesion. Additionally, it should be noted that the occurrences of the pull-in and pull-off events are abrupt and take an average time of less than 17.18 ms.

TABLE I

EXPERIMENTAL DATA AND ANALYSIS OF THE ESTIMATED PULL-IN AND PULL-OFF FORCES DURING AFM TIP-$LiNbO_3$ SAMPLE INTERACTION.

Test	Mean	std	1	2	3	4	5	6	7	8	9	10
Pull-in force (pN)	-0.91	0.13	-0.82	-0.69	-1.11	-1.14	-0.79	-0.92	-0.84	-0.9	-0.98	-0.9
Pull-in time (ms)	17.18	8.4	24	7.2	12.4	4.7	20.4	16.8	30	26.4	19.2	10.7
Position(μm)	1.49	0.013	1.48	1.5	1.49	1.5	1.47	1.49	1.49	1.48	1.51	1.48
Pull-off force (pN)	-16.79	3.05	-21.76	-20.57	-19.59	-17.88	-18.35	-14.86	-14.25	-13.56	-13	-14.09
Pull-off time (ms)	16.5	7.3	6	27.5	20.4	13.2	21.6	4.8	21.6	12	18	20.3
Position (μm)	1.34	0.031	1.29	1.32	1.32	1.35	1.32	1.35	1.36	1.36	1.41	1.36

B. Study on the behavior of microdisk-sample interaction

The key concern of this section is to understand the interaction behavior of the microdisk with the waveguide. For the analysis, a 50 μm diameter microdisk with a thickness of ∼1 μm is assembled under SEM at the tip of an AFM cantilever. This raises key questions by changing the contact area and also the added mass on the cantilever. Therefore, a comparison of the behavior of this configuration with that of a regular AFM tip is investigated.

A similar procedure is used to plot force-distance curves as in regular AFM tip-sample interaction. Fig. 8 shows 10 force-displacement curves generated when the sample is approached to the microdisk. The respective pull-in and pull-off data are recorded in table II.

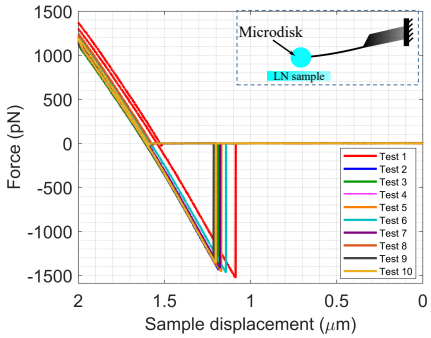


Fig. 8. Experimental results showing 10 force-displacement curves used in the estimation of pull-in and pull-off forces during microdisk/LN sample interaction.

The value of the adhesion force is ∼45 times higher than the pull-in forces. Additionally, the contact detection repeatability, when the pull-in force is maximum, is achieved with a standard deviation of 23 nm, showing high accuracy repeatability.

C. Optical response mapping for microdisk-waveguide interaction

Optical quantification through controlled X–Y scanning at a constant disk–substrate separation enables precise identification of the lateral position that maximizes the resonance response, thereby improving positioning accuracy and enabling in-situ optical characterization. Therefore, the optical response of the waveguide is mapped as the microdisk is scanned in the X-Y plane using a high-precision nanopositioner. The waveguide, approximately 7 μm wide, is scanned over a 30 × 30 μm area with step sizes of 5 μm along X and 1 μm along Y. Initially, the AFM Z-axis is fully extended. During mapping, the AFM XYZ piezo positioner is fully extended along the Z-axis, ensuring that the microdisk does not initially contact the waveguide. Under these conditions, the laser intensity of the Position-Sensitive Detector (PSD) is set to I = 0. A closed-loop control is activated that maintains the laser intensity at 0.5 nA, and the nanopositioner is then brought closer to the sample until the AFM's piezo positioner begins to retract, ensuring a constant interaction force at this intensity.

At each scan point, transmission and reflection spectra are recorded for quasi-TE and quasi-TM modes over the 1530–1550 nm wavelength range, with each spectral acquisition taking approximately 1 minute. After each measurement, the waveguide is retracted along the Z-axis to prevent surface damage before moving to the next Y-position. This process is repeated systematically across the defined scan area to fully characterize the optical interaction between the microdisk and the waveguide on the X-Y plane.

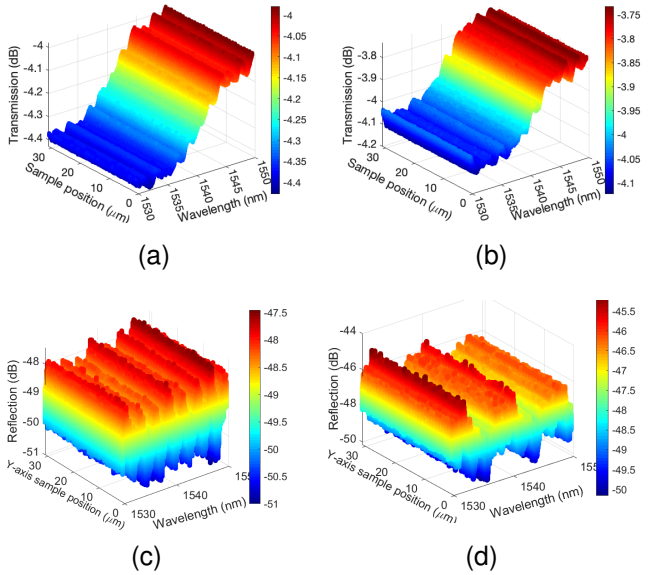


Fig. 9. Experimental results showing 3D map of the optical response (Transmission and reflection spectra for Transverse Electric (TE) and Transverse Magnetic (TM) modes) of the waveguide, with the microdisk on its surface with a controlled contact force, while scanning along its Y-axis. (a) 3D map of the transmission spectra for TM mode. (b) 3D map of the transmission spectra for TE mode. (c) 3D map of the reflection spectra for TM mode. (d) 3D map of the reflection spectra for TE mode.

Fig. 9 presents a set of 3D spectral maps illustrating the optical response of the waveguide along the Y-axis. The recorded spectra confirm that all 30 measurements exhibit minimal losses, indicating a stable interaction between the waveguide and the microdisk. The standard deviation of the

TABLE II

EXPERIMENTAL DATA AND ANALYSIS OF THE ESTIMATED PULL-IN AND PULL-OFF FORCES DURING MICRODISK-$LiNbO_3$ SAMPLE INTERACTION.

Test	Mean	std	1	2	3	4	5	6	7	8	9	10
Pull-in force (pN)	-31.22	3.27	-33.49	-37.29	-30.78	-32.68	-32.27	-32.68	-29.42	-28.39	-30.92	-24.27
Pull-in time (ms)	9.6	3.3	10.8	09.6	13.2	7.2	9.6	2.4	12.0	13.2	10.8	7.2
Position (μm)	1.57	0.023	1.52	1.58	1.60	1.59	1.58	1.58	1.59	1.57	1.59	1.59
Pull-off force (pN)	-1421	55	-1528	-1441	-1413	-1412	-1459	-1468	-1417	-1384	-1324	-1362
Pull-off time (ms)	12.0	5.4	10.7	22.8	7.2	6.0	13.1	13.2	16.8	10.7	14.4	4.8
Position (μm)	1.17	0.035	1.09	1.18	1.19	1.18	1.17	1.14	1.18	1.2	1.22	1.20

transmission signal at 1530 nm for TE and TM is 0.001766 dB and 0.002241 dB, respectively. Furthermore, these results demonstrate that the proposed positioning strategy enables a precise spectral reconstruction of the waveguide–microdisk interaction. This approach, leveraging a standard AFM in static mode, allows for controlled-force optical mapping in three dimensions and dual polarization, a key advantage for high-resolution optical characterization.

VI. CONCLUSION

This study investigates the interaction between a microdisk and a waveguide surface using AFM force-displacement measurements to quantify the pull-in and pull-off forces during approach and retraction. The experimental results show a pull-in force of 37.29 pN and a significantly larger pull-off force of up to 1.5 nN, which is approximately 40 times higher due to adhesion effects. Compared with a conventional AFM tip (tip radius $\sim$10 nm), the use of a microdisk (50 μm diameter and 1 μm thickness) increases the pull-in and pull-off forces by approximately 35 times and 85 times, respectively. This increase is mainly attributed to the larger interaction area and capillary adhesion when operating in air.

The pull-in transition occurs rapidly ($<$10 ms), resulting in a sudden switch from non-contact to contact, which complicates static AFM control during close positioning. However, the repeatability of the pull-in position is about 23 nm, indicating that pull-in detection can be used for high-accuracy positioning.

To address the alignment challenge, a 3D positioning strategy is proposed through modifications to the fabrication of the waveguide's electrodes. A visualization window is integrated into the membrane to enable optical observation of the microdisk through the waveguide, together with position markers to facilitate precise alignment. The combination of an XYZ-axis nanopositioner and AFM closed-loop positioning with laser intensity feedback enables controlled-force positioning of the microdisk on the waveguide surface during spectral response analysis.

In summary, this study demonstrates a generic method for both active and passive robotic positioning of microcomponents by leveraging the effectiveness of AFM in assembly procedures and analysis.

REFERENCES

[1] J. Wang and Q. Zou, "Rapid probe engagement and withdrawal with force minimization in atomic force microscopy: A learning-based online-searching approach," *IEEE/ASME Transactions on Mechatronics*, vol. 25, no. 2, pp. 581–593, 2020.

[2] J. Yi, W. Haouas, M. Gauthier, and K. Rabenorosoa, "A pdms/silicon adhesion control method at millimeter-scale based on microvibration," *Advanced Intelligent Systems*, vol. 7, no. 2400394, 09 2024.

[3] Y. Zhang, B. K. Chen, X. Liu, and Y. Sun, "Autonomous robotic pick-and-place of microobjects," *IEEE transactions on robotics*, vol. 26, no. 1, pp. 200–207, 2009.

[4] J. Hou, C. Wu, Z. Wang, S. Yuan, P. Yu, and T. Liu, "Afm nanomanipulation with tip morphology estimation and positioning compensation," in *Int. Conf. on Nano/Micro Engineered and Molecular Systems*, 2019, pp. 534–539.

[5] S. Liu, Y.-F. Li, and X.-W. Wang, "A novel dual-probe-based micrograsping system allowing dexterous 3-d orientation adjustment," *IEEE Transactions on Automation Science and Engineering*, vol. 17, no. 4, pp. 2048–2062, 2020.

[6] B. Tiwari, C. Clévy, and P. Lutz, "High-precision gluing tasks based on thick films of glue and a microrobotics approach," *IEEE Robotics and Automation Letters*, vol. 4, no. 4, pp. 4370–4377, 2019.

[7] B. Komati, C. Clévy, and P. Lutz, "Sliding mode impedance controlled smart fingered microgripper for automated grasp and release tasks at the microscale," in *Int. precision assembly seminar*. Springer, 2018, pp. 201–213.

[8] A. Awde, M. Boudaoud, M. Macioce, S. Régnier, and C. Clévy, "A microrobotic approach for the intuitive assembly of industrial electrooptical sensors based on closed-loop light feeling," *IEEE/ASME Transactions on Mechatronics*, vol. 27, no. 6, pp. 5462–5471, 2022.

[9] H. Bettahar, O. Lehmann, C. Clévy, N. Courjal, and P. Lutz, "6-dof full robotic calibration based on 1-d interferometric measurements for microscale and nanoscale applications," *IEEE Trans. on Automation Science and Engineering*, vol. 19, no. 1, pp. 348–359, 2020.

[10] H. Bettahar, C. Clévy, N. Courjal, and P. Lutz, "Force-position photorobotic approach for the high-accurate micro-assembly of photonic devices," *IEEE Robotics and Automation Letters*, vol. 5, no. 4, pp. 6396–6402, 2020.

[11] H. Xie and S. Régnier, "Three-dimensional automated micromanipulation using a nanotip gripper with multi-feedback," *J. of Micromechanics and Microengineering*, vol. 19, no. 7, p. 075009, 2009.

[12] F. R. Leiro, S. Régnier, S. Haliyo, and M. Boudaoud, "A robotic strategy for in-plane center of rotation identification and control in atomic force microscopy," *IEEE Robotics and Automation Letters*, vol. 9, no. 1, pp. 523–530, 2024.

[13] Z. Sun, N. Xi, Y. Xue, Y. Cheng, L. Chen, R. Yang, and B. Song, "Task space motion control for afm-based nanorobot using optimal and ultralimit archimedean spiral local scan," *IEEE Robotics and Automation Letters*, vol. 5, no. 2, pp. 282–289, 2020.

[14] T. Kim, D. Kim, T. Kim, H. Kim, and C. Shin, "Advanced hybrid positioning system of sem and afm for 2d material surface metrology," *Microscopy and Microanalysis*, vol. 28, no. 5, pp. 1604–1610, 10 2022. [Online]. Available: https://doi.org/10.1017/S1431927622000903

[15] M. Mwangi, F. Behague, A. Coste, J. Safioui, M. Suarez, J. Byiringiro, P. Lutz, C. Clévy, and N. Courjal, "In-situ phase control of a low-loss polarisation-state modulator," *Optics Continuum*, vol. 1, no. 12, pp. 2513–2520, 2022.

[16] B. Pan, H. Cao, Y. Huang, Z. Wang, K. Chen, H. Li, Z. Yu, and D. Dai, "Compact electro-optic modulator on lithium niobate," *Photonics Research*, vol. 10, no. 3, pp. 697–702, 2022.